Numerical investigation of auto-ignition length and wall heat flux for near-wall reaction of CH4

Conference Paper · September 2021

CITATION
1

READS
59

4 authors, including:

Paola Breda
HyImpulse GmbH
21 PUBLICATIONS **58** CITATIONS
SEE PROFILE

Lukas Fischer
Universität der Bundeswehr München
3 PUBLICATIONS **2** CITATIONS
SEE PROFILE

Michael Pfitzner
Universität der Bundeswehr München
294 PUBLICATIONS **2,095** CITATIONS
SEE PROFILE

Numerical investigation of auto-ignition length and wall heat flux for near-wall reaction of CH_4

P. Breda[1*], L. Fischer[1], R. Dalshad[1] and M. Pfitzner[1]

*paola.breda@unibw.de

[1] *Institut für Thermodynamik, Universität der Bundeswehr München, Werner-Heisenberg-Weg 39, 85577 Neubiberg*

Abstract

Reactive Large Eddy Simulations (LES) with direct integration of chemistry are presented in this work for the numerical investigation of a novel test bench developed at the Bundeswehr University of Munich. The experimental setup aims to investigate secondary near-wall reactions caused by cold fuel injection into a hot crossflow and it provides measurements of OH-PLIF, OH* and reconstructed wall heat fluxes for comparison with numerical computations. Here the experimental configuration with methane as fuel and an impulse ratio of 10 is investigated. The effect of chemistry is investigated using two reduced chemical mechanisms with 19 and 30 species, respectively. Two meshes including one and three fuel injector nozzles are considered, to investigate the jet-to-jet interaction. Four inlet temperatures for the hot flows are investigated, to estimate the sensitivity of the autoignition length to a variation of the hot inlet temperature. The results show that the autoignition length estimated from the OH and CH_2O concentrations is strongly dependent on the temperature of the hot reactants and that chemistry is the driving factor to trigger autoignition in the chosen configuration. A qualitatively good approximation with the experimental autoignition length is obtained with a hot inlet temperature of 1600-1620 K. The numerical wall heat flux does not predict the local peak due to the reaction zone close to the wall, but the order of magnitude of the experiment is reached.

Introduction

Thermal components for gas turbines or combustion chambers are usually dimensioned to operate above their structural limit to increase the combustion efficiency. Cooling techniques are therefore required to prevent thermal damage. The recent development of Ultra Compact Combustors (UCC) to increase the combustion efficiency by increasing the residence time is often accompanied by incomplete combustion which causes the presence of unburned fuel-rich mixtures downstream the combustion chamber. The interaction with the coolant flow at the turbine blades could trigger local autoignition and subsequent secondary reactions near the blade surface, leading to an incremental heat flux towards the blade. Kirk, Lukachko and coworkers [1][2] estimated an increase in wall heat flux up to 25% when a reactive boundary layer establishes, compared to a non-reactive configuration.

Secondary reactions were thoroughly investigated at the experimental test bench of the Air Force Research Laboratory (AFRL) and the results presented in several publication e.g., [3][4]. Air was injected into a crossflow of fuel rich C_3H_8/air combustion gases and various film cooling configurations were investigated. Planar Laser-Induced Fluorescence (PLIF) measurements of CO and OH allowed to observe the secondary reaction zone for different blowing ratios. Mixing between crossflows at the same test bench was numerically investigated [5] using a 2-step mechanism for C_3H_8. The impact of variable geometry and allocation of the coolant holes was also investigated with RANS [6]. Pohl et al. [7] investigated a modified configuration of this test bench in RANS to determine the impact of the trench and film cooling. Frank [8] used the same experiment to validate tabulated frozen chemistry tables. A limiting factor of this test bench was that the limited number of thermocouples at wall could not provide an insight of the wall heat flux distribution and therefore it could not be used for the validation of CFD combustion models.

Motivated by the need for further understanding secondary combustion and to provide experimental data for numerical validations, a novel test bench was recently developed at the Bundeswehr University of Munich by Dalshad et al. [9]. The configuration is opposite to the test bench of Evans: cold fuel (CH_4, H_2 or C_3H_8) is injected into an oxygen-rich hot exhaust crossflow. Two fuel injection configurations were investigated with an angle of respectively 90° and 30° with the crossflow [9][10]. PLIF

measurements of OH and OH* chemiluminescence images allowed to locate the reaction zone and to qualitatively estimate the autoignition length across several configurations. Reconstructed wall heat fluxes are available from the inverse heat transfer problem [11]. Because this test bench is relatively new, no numerical investigations are available in the literature yet. One of the main challenges is the determination of plausible boundary conditions for the CFD, because of the uncertainties on the hot crossflow composition and the difficult access of 2D measurements. The hot flow inlet temperature distribution is also not homogeneous and it was seen to vary between 1500 and 1620 K [9]. A more detailed paper from the authors reports the assessment of the boundary conditions for Large Eddy Simulations (LES) using a selected configuration of this test bench with methane as fuel [12]. The choice of LES allows to get an insight of the flow unsteadiness in the burner and at the hot gas inlet. The experimental configuration features a partially premixed flame with an autoignition delay (or lifted flame). For this purpose, the laminar chemistry approach is chosen for LES, where the criterion of Pope on the turbulent kinetic energy [13] is satisfied on the numerical grids. The effects of varying the grid refinement, the chemical mechanism, the turbulent inlet and the hot gas inlet temperatures as well as the interaction between the fuel jets are presented in this work.

Governing Equations

The LES transport equations used in the OpenFOAM solver are briefly discussed in this paragraph. The Navier-Stokes equations for density-variable flows are filtered in LES by the local filter width Δ which is calculated from the cell volumes of the computational mesh. The mass and momentum equations read

$$\frac{\partial \bar{\rho}}{\partial t} + \frac{\partial \bar{\rho}\widetilde{u_i}}{\partial x_i} = 0 \tag{1}$$

$$\frac{\partial \bar{\rho}\widetilde{u_i}}{\partial t} + \frac{\partial \bar{\rho}\widetilde{u_i}\widetilde{u_j}}{\partial x_j} = -\frac{\partial \bar{p}}{\partial x_i} + \frac{\partial}{\partial x_i}\left(\bar{\tau}_{ij} - \bar{\rho}\left(\widetilde{u_i u_j} - \widetilde{u_i}\widetilde{u_j}\right)\right). \tag{2}$$

The bar sign indicates the LES filtered quantities like the pressure $\bar{p}$ and the density $\bar{\rho}$, while the tilde sign reports the Favre-averaged quantities like the *i-th* component of the velocity $\widetilde{u_i}$.The hypothesis of Newtonian fluids is used for shear-stress tensor which becomes $\bar{\tau}_{ij} = 2\bar{\mu}(\tilde{S}_{ij} - 1/3\delta_{kk}\tilde{S}_{kk})$ and shows a proportionality to the rate-of-strain tensor $\tilde{S}_{ij} = \frac{1}{2}(\frac{\partial \widetilde{u_i}}{\partial x_j} + \frac{\partial \widetilde{u_j}}{\partial x_i})$, with μ being the dynamic viscosity. The Reynolds stresses $\left(\widetilde{u_i u_j} - \widetilde{u_i}\widetilde{u_j}\right)$ are closed similarly to $\bar{\tau}_{ij}$ by replacing the filtered $\bar{\mu}$ with the turbulent viscosity μ_t (Boussinesq hypothesis). The latter is modelled by the Wall-Adapting Local Model Eddy-viscosity (WALE) model for wall-bounded LES [14].

To correctly describe the autoignition problem of the experiment, finite rate chemistry LES were considered, which require at least 15 species to describe autoignition of methane. The reactive LES requires the transport of (n_s – 1) equations for the n_s species of the selected chemical mechanisms, treating nitrogen as inert species. The transport equation for the *k* species can be written as follows, under the assumption of unity Lewis numbers:

$$\frac{\partial \bar{\rho}\widetilde{Y_k}}{\partial t} + \frac{\partial \bar{\rho}\widetilde{Y_k}}{\partial x_i} = \frac{\partial}{\partial x_i}\left(\frac{\bar{\mu}}{Sc}\frac{\partial \widetilde{Y_k}}{\partial x_i} + \frac{\mu_t}{Sc_t}\frac{\partial \widetilde{Y_k}}{\partial x_i}\right) + \overline{\dot{\omega}}_k . \tag{3}$$

Y_k is the species mass fraction, $\overline{\dot{\omega}}_k$the filtered source term of species *k* and *Sc* the Schmidt number for the molecular and turbulent mass transport. A value of 0.7 is assigned according to previous investigations. The filtered source term appears in unclosed form and usually requires modelling to correctly describe the Turbulence-Chemistry Interaction (TCI) on the LES sub-grid scales. Following the results obtained in previous investigations [15][16][17], the laminar chemistry assumption is used in this work, meaning that the source terms are directly calculated using the filtered $\widetilde{Y_k}$ and $\tilde{T}$ in the Arrhenius equations.

In addition to the species transport, the energy equation is written in terms of sensible enthalpy h_s and for unity Lewis numbers as

$$\frac{\partial \bar{\rho}\widetilde{h_s}}{\partial t} + \frac{\partial \bar{\rho}\widetilde{h_s}}{\partial x_i} = \frac{\partial}{\partial x_i}\left(\frac{\bar{\mu}}{Pr}\frac{\partial \widetilde{h_s}}{\partial x_i} + \frac{\mu_t}{Pr_t}\frac{\partial \widetilde{h_s}}{\partial x_i}\right) + \bar{\dot{\omega}}_T \quad (4)$$

where the terms containing the viscous heating and the pressure fluctuations were neglected because of the range of applicability of this test case (low Mach numbers). The Prandtl number *Pr* describes the molecular transport in terms of heat conduction and its value is also equal to 0.7. The enthalpy source term is formed from the knowledge of the chemical source terms $\bar{\dot{\omega}}_k$and the standard enthalpy of formation Δh_0^k. The transport properties for the mixture are calculated using the Sutherland model while the density if calculated from the equation of state for ideal gases.

Test Case

Dalshad et al. [9] investigated secondary reactions in proximity of cooled walls using a jet-crossflow configuration. The oxygen-rich hot crossflow is provided by a gas generator [10], whereas the coolant is either CH_4, H_2 or C_3H_8. The coolant can be injected at different momentum ratios through 5 nozzles of diameter 0.4 mm, at an angle of 30° to the crossflow direction, as shown in Figure 1.

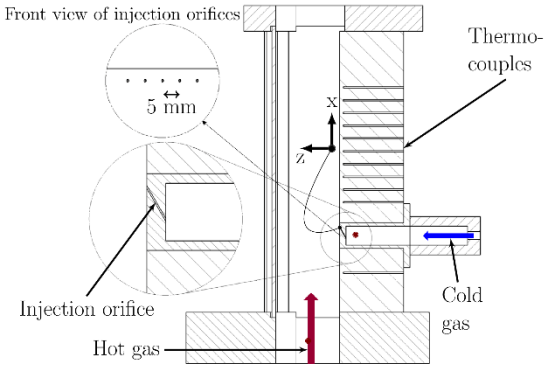

Figure 1. Cross-sectional view of the reactive test section.

An experimental configuration allowing for a stable reaction zone is chosen for the CFD validation, to identify where autoignition triggers. Pure CH_4 is chosen as coolant, with a momentum ratio of I=10, based on a mean jet velocity of U_c = 86 m/s and a bulk crossflow velocity U_h =27 m/s. The higher the momentum I, the higher is the penetration depth of the coolant into the main flow and the more stabilized appears the secondary combustion zone [9]. The hot gas composition was determined using 0D-reactor models available in Cantera [10] and it is summarized in Table 1, together with the remaining boundary conditions.

Table 1. Boundary conditions retrieved from the experiment.

Inlet	U [m/s]	Re	T [K]	Composition
Hot flow (*h*)	27	5070	1500, 1550, 1600, 1620	Y_{O2} = 0.0842 Y_{N2} = 0.7401 Y_{H2O} = 0.0789 Y_{CO2} = 0.0966
Cold fuel (*c*)	86	599	570	Y_{CH4} = 1

After the reactants mix, chemical activity is observed within the test section. The experiment is equipped with a laser to detect Planar Laser Induced Fluorescence (PLIF) of OH and an example of selected post-processed images is shown in Figure 2. The left side shows a snapshot of OH at the generic time t_i while the right side shows an average over 300 images. The data acquisition techniques and the postprocessing steps are reported in detail in [9]. Two reaction zones are detected by the laser throughout the flame: the lower flame branch due to the interaction of the fuel core with the cooled wall, and the upper flame branch due to the interaction of the fuel core with the hot gases. The same criterion used in [10] was used to qualitatively estimate the experimental autoignition length for this configuration, based on a 3%

increase of OH in the radical pool. The flame tip is located at an estimated length of L_{ig} = 40.8 mm from the fuel injector nozzles.

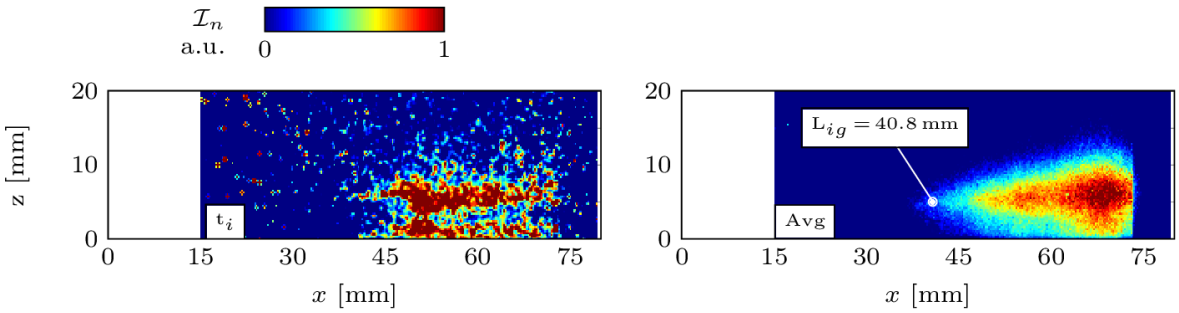

Figure 2. Left: instantaneous OH-PLIF acquisition. Right: average OH-PLIF.

Because the reaction zone is located at the wall proximity, this segment is capacitively cooled using a water manifold. Experimental data for the wall heat flux are provided by means of the inverse heat transfer problem, based on 11 thermocouple readings available at the cooled wall [11].

Numerical Setup

Two sufficiently refined LES meshes were generated to investigate the effects of the chemical mechanism, the jet/jet interaction and temperature variation at the hot inlet. Being x, y, z the streamwise, spanwise and the wall normal directions, the first computational domain has dimensions 82x5x20 mm^3 and $0.98*10^6$ (0.98M) volume cells and it includes one injector only. The second mesh has dimensions 165x15x20 mm^3 with 2.1M cells including three injectors. These meshes are labelled respectively M1 and M2. The upper wall is treated as symmetry plane. The spanwise patches are treated as periodic boundary conditions. For both meshes, the maximum y^+ detected at wall is about 5.3, with an average value of 1.1. A maximum grid size of Δ = 0.61 mm is found at the top wall close to the outlet in M2, while it is confined below 0.3 mm where the flame is located. Similar values are retrieved from M1. In both domains, the CH_4 injector slots are located about 4 mm downstream the hot flow inlet. Constant values are applied at the fuel inlet as shown in Table 1. Artificial turbulence is applied at the hot inlet in one configuration, using the digital filters method [18]. The determination of the boundary conditions for the reactive LES are discussed in detail in a separate work [12]. The wall temperature is interpolated from the experimental values, obtained from the thermocouples' readings.

The momentum and pressure equations for the OpenFOAM solver are coupled with a PISO loop. The time integration scheme is an implicit Euler first order, while a van Leer second order is used for the scalar diffusion terms. A second order unbounded Gauss linear scheme is used for the velocity instead because less dissipative. The time step is adjusted at runtime to provide CFL = 0.6. The LES averaged fields are calculated over about 5 flow-through times.

Table 2. Investigated LES configurations.

Case	Mesh-Chemistry-Injectors	T_h [K]	Turbulent Inlet
C1	M1-Lu30-1	1500, 1550, 1600, 1620	-
C2	M2-Lu19-3	1500, 1550, 1600, 1620	-
C3	M1-Lu30-1	1620	Digital filters
C4	M2-Lu19-3	1620	Digital filters

Table 2 summarizes the investigated numerical setups. C1 and C2 are based on finite rate chemistry computations without TCI modelling on the subgrid, using the mechanisms Lu30 [19] and Lu19 [20] with respectively 30 and 19 species. The autoignition length is first investigated neglecting turbulence at the inlet, considering four different T_h. This is because the experimental data revealed a rather inhomogeneous temperature distribution at the hot exhaust gases coming from the burner. A peak value

of 1620 K was reconstructed from the experiment, while the thermocouples located at the inlet perimeter reported readings localized around 1500-1600K [9]. The fuel inlet is assigned a mean temperature of 570 K. This evaluation derived from a previous LES of the CH_4 injector nozzle, considering the heating of the fuel from the tank (ambient temperature) to the injection plate [12]. C3 and C4 correspond to configurations C1 and C2 with T_h =1620K and artificial turbulence applied at the hot inlet.

Results

The effects of changing the hot gas inlet temperature on the autoignition length is first discussed using the configurations without turbulent boundary conditions of Table 2. The left column of Figure 3 shows an axial cut on the central plane (y = 0) colored by the mean temperature field. In each figure, the top half represents configuration C1, the bottom half C2. For T_h = 1500 K no visible flame ignition is observed in C1 because the domain is too short. In fact, a stronger temperature gradient is observed in C2 from about x > 80 mm. By increasing T_h the flame tip moves further upstream, as frequently observed in the literature for similar flame configurations [21]. In fact, the location of the autoignition kernel strongly depends on the temperature of the hot reactants, in this case the oxidizer inlet. A temperature increase also increases the rate of reaction, promoting the fast chemistry process. The lifted flame of this test case establishes because the reaction/diffusion process within the ignition kernel balances the convective force, which would otherwise transport the kernel outside the domain. By further increasing the temperature, the flame anchoring point shifts further upstream until an attached flame can be observed at the fuel injector nozzle. It is also interesting to notice the presence of a double branch of the flame, as also observed in the snapshot of OH-PLIF shown in Figure 2. The lower branch of the flame appears for higher inlet temperatures. The upper flame derives from the mixing and reaction of the methane core with the hot coflow, while the bottom flame is located where the methane-enriched mixture reacts with the oxidizer stream, the latter being cooled down by the wall.

If artificial turbulence is provided at the hot inlet for the case at T_h = 1620 K (configurations C3 and C4 on the bottom left plot) the flame tip shifts upstream of about 6 mm compared to the configurations C1-C2. A stronger shift is observed for C4, featuring three injection nozzles. Although there is an effect of enhanced mixing created by the turbulent content at the oxidizer inlet, the autoignition point does not significantly move within the domain. In this configuration, the effect of chemistry appears to be stronger than turbulence. This is mainly due to the high momentum ratio (I=10) featuring an increased jet penetration into the crossflow and the relatively high temperature of the oxidizer stream.

A qualitative assessment of the autoignition length in the numerical simulations can be provided by the OH and the CH_2O concentrations. In this work only the OH can be compared with the experimental OH-PLIF, while species CH_2O is often used as indicator of autoignition based on the radical pool forming during the induction time. In both cases, the OH and CH_2O concentrations are first integrated over the line of sight (the *y*-axis). Since the meshes have different depths, the fields are sampled over 100 slices in *y* for C1 and 300 slices for C2. The integration of the obtained images is performed with a Phyton processing tool and normalized between 0 and 1. The final images are shown in black and white for mesh C2 on the right column of Figure 3. The OH integration allows to detect the flame throughout its depth, as shown by the gray region between the two flame branches. This region also locates the pool of radicals building prior autoignition, identified by species CH_2O in the numerical simulations. It is clear to see from each image that the radical pool always initiates before the OH formation, where the temperature is still close to the fuel core temperature. The difference between the starting locations of the CH_2O and OH reaction zones reduces by increasing T_h. This is because the chemistry is more reactive at higher temperatures, leading to a shorter induction zone. The integrated CH_2O also detects the presence of the double flame. Additionally, chemical activity is shown at the wall proximity due to the Flame-Wall Interaction (FWI).

Two autoignition criteria are chosen to estimate the autoignition length, namely a 3% increase in OH and a 10% increase in CH_2O. To apply the criterion on a 1D distribution, the OH and CH_2O post-processed images of Figure 3 are integrated along the *z*-axis. To be consistent with the experimental evaluation of [10], the pixel intensities from the black/white images are added together along the *z* -axis, providing a unique distribution along the *x*-axis. The integrated curves are labelled as $\int Y\, dz$ in Figure 4 and are shown in red for C1 and in black for C2. The left column shows the autoignition length calculated for OH ($L_{3\%OH}$) while the right column shows the calculation for CH_2O ($L_{10\%CH2O}$). The correspondent autoignition points are marked by the symbols and reported in Table 3 in mm.

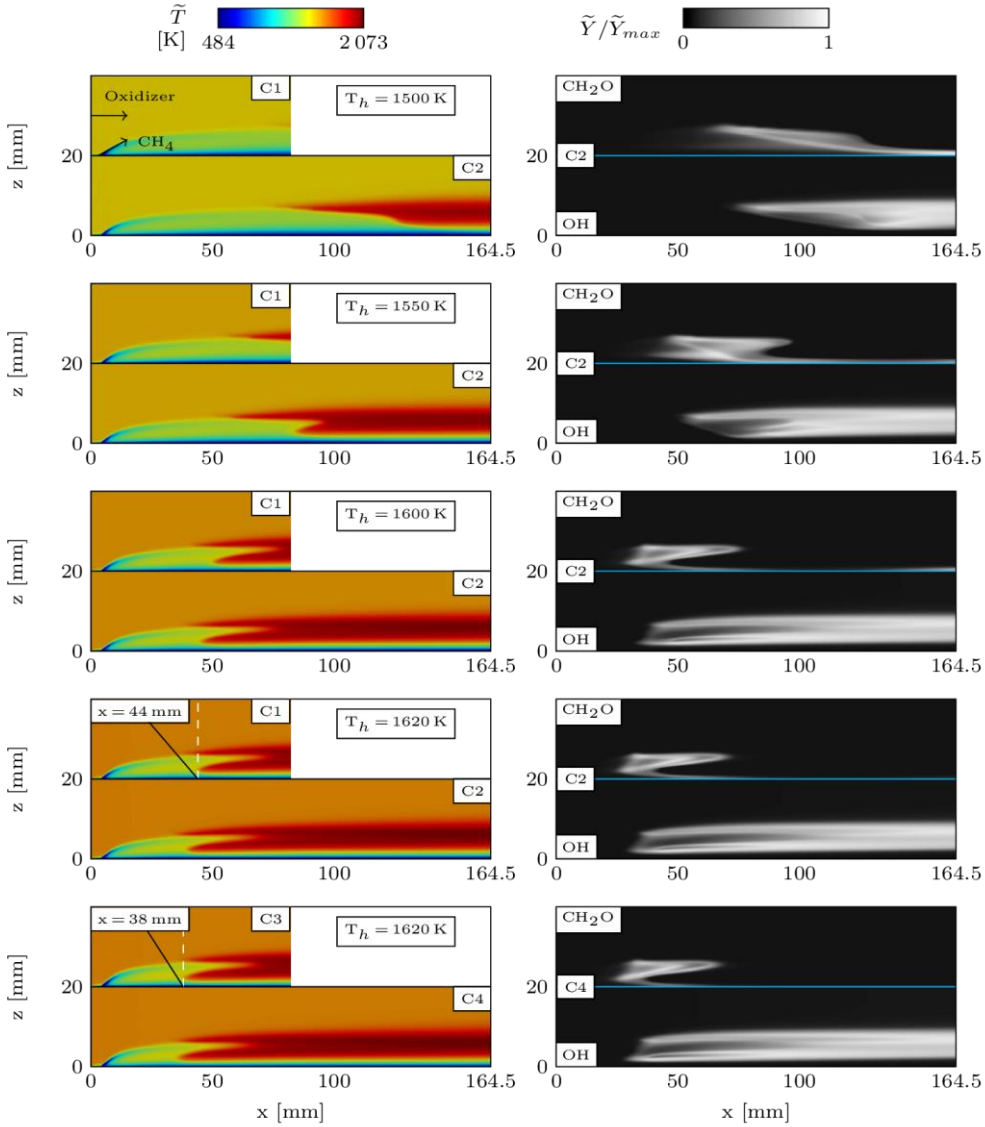

Figure 3. Left: center line cut for T field. Right: line-of-sight integration of OH and CH_2O. Configurations of Table 2.

When using CH_2O to detect autoignition, the autoignition length is shifted upstream compared to the OH criterion, the difference decreasing by increasing T_h. Looking at the table columns for $L_{10\%CH2O}$, a minimal difference is observed between C1 and C2, the difference becoming stronger when calculating $L_{3\%OH}$. When a turbulent content is provided at inlet, the ignition length is reduced of about 2 mm in the respective configurations (thus, from C1 to C3 and from C2 to C4). The integrated OH retrieved from the experimental image (Figure 2 on the right) is shown by the cyan curve, corresponding to an autoignition length of 40.8 mm. According to the table, the CFD simulations at T_h =1600 K can better represent this value based on the OH criterion.

A qualitative observation of the flame position in Figure 3 shows that in C2 the flame is always shifted upstream a couple of centimeters compared to C1 (see for example T_h =1620 K). This is also confirmed by the calculated $L_{3\%OH}$. Three factors can influence this behavior: the chemical mechanisms, the meshing and/or the interaction between jets. The numerical BCs generate only minor turbulence in the chosen configuration and chemistry appears to be the driving mechanisms for autoignition. However, a 0D-reactor analysis shows that the Lu19 chemistry can correctly represent the autoignition times of Lu30 (cf. Fig. 7 in [16]). Therefore, the injector/injector interaction as well as the different meshing could be responsible for the anticipated ignition in C2.

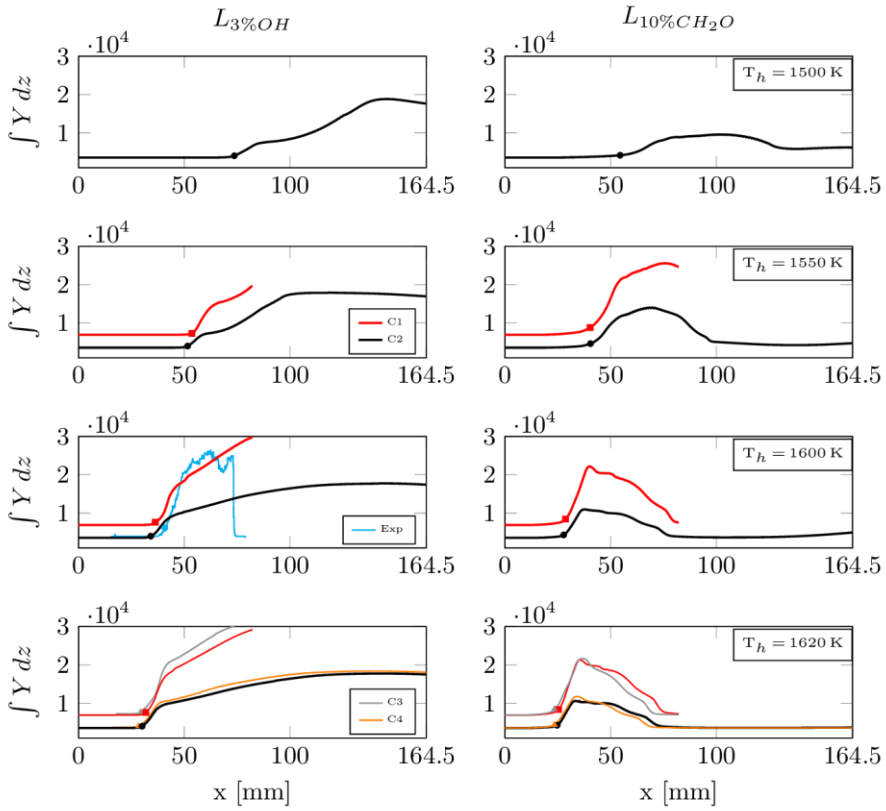

Figure 4. Integration along the *z*-axis of the OH and CH_2O pixel distributions from the black/white images of Figure 3.

Table 3. Autoignition lengths.

	$L_{3\%OH}$ [mm]				$L_{10\%CH2O}$ [mm]			
T_h [K]	C1	C2	C3	C4	C1	C2	C3	C4
1500	-	73.7	-	-	-	54.5	-	-
1550	53.7	51.6	-	-	40.3	40.5	-	-
1600	36.3	34.1	-	-	28.7	27.8	-	-
1620	31.8	30.1	29.4	28.3	24.7	24.7	23.6	23.4

A cut section through the jet cores at z = 6 mm is shown for T_h =1550 K in Figure 5 and qualitatively confirms this observation. While the length of the central jet remains approximately the same when moving to the 3-injector configuration, a different core length is observed for the external jets. Overall, the fuel jets seem to complete mixing with the crossflow earlier in the domain for the 3-injectors configuration.

Another interesting insight provided by the numerical simulations is the justification of the lower flame branch observed in Figure 3. In fact, an entrainment of hot oxidizer is forced between the fuel-rich jet and the cold gases at wall, where the radical pool is forming (cf. x = 30 mm in Figure 3). In this region a strong production of CH_2O is observed while the temperature remains almost constant and close to the hot oxidizer temperature. The reason why this entrainment is creating is due to the presence of vortical structures in the fuel jet. This phenomenon is illustrated for clarity in Figure 6, where the slices normal to the hot crossflow show the temperature field, while the two counter-rotating jets are colored by the transversal velocity $\widetilde{U}_y$ to highlight the directions of rotation. It is clear to see that the vortical motions transport hot gases from the top to the bottom of the jets, creating the recirculation zone leading to the formation of the lower flame branch.

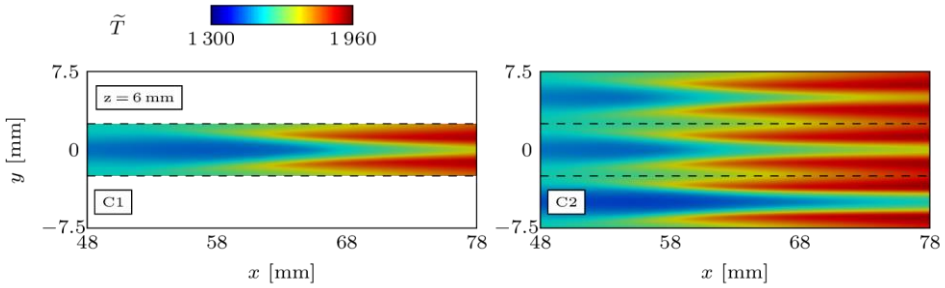

Figure 5. Cut across the methane jets at z = 6 mm for configurations C1 and C2.

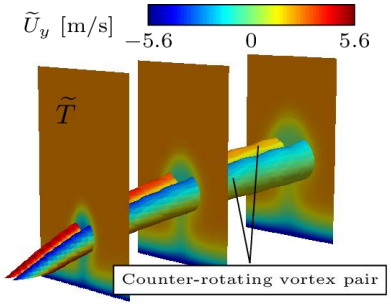

Figure 6. Counter-rotating vortex structure of the fuel jet.

The second quantity of comparison with the experiment is the wall heat flux, whose experimental value was reconstructed from the inverse heat transfer problem using the thermocouple readings [11]. The position of the thermocouples at the wall is shown by the black dots on the bottom right of Figure 7, together with the computational domains of C1 and C2 (in gray). The locations of the fuel injectors are reported for completeness. The reconstructed 2D distribution of q_w from COMSOL [11] is interpolated at the wall patches of meshes C1 and C2, to integrate on the same grid.

The numerical wall heat flux is calculated as $\tilde{q}_w = (\bar{\lambda} + \lambda_t)\nabla\tilde{T}$ and since the meshes are wall-resolved, it is $\lambda_t \sim 0$. An integration of the experimental and numerical q_w along the *y*-axis is performed to allow the comparison on the 1D axial profile only. The integration is performed over 100 equally distributed axial points x_i for mesh C1 (200 points for mesh C2) and between locations x_1 = 5.1 mm and x_2 = 82.3 mm (164.5 mm for C2). Note that x_1 is selected after the fuel injection slot. Figure 7 summarizes the results for C1 (top left) and C2 (top right). The experimental curve shows a rather constant heat flux, with a local peak achieved between 60 and 70 mm downstream the injectors. The peak detects the reaction zone at the wall proximity. The numerical simulations report smoother local peaks, whose location depends on the temperature of the hot oxidizer. There is a high local peak predicted by the simulations right after the injectors, which is not seen by the experiment. The fact that no thermocouple readings are available for x < 25 mm could provide some uncertainties in the experimental wall heat flux prediction in this range. As fuel and oxidizer mix, the q_w sinks downstream the injectors.

The bottom left plot shows the thermal boundary layer developing at the center line, sampled respectively 0.5, 1, 2 and 3 mm from the wall for case C1 at T_h =1620 K. The temperature evolution from 0.5 to 3mm shows where the fuel core is located, at the point of temperature drop. The temperature profiles detect the presence of the flame, with a steep gradient located at x = 40 mm starting from z > 1 mm from the wall. This corresponds to a local maximum in q_w for this configuration (cf. gray solid curve). Such local peaks can be identified for T_h =1500 K and 1550 K in the second half of the domain (cf. C2). For T_h = 1600 K and 1620 K instead the peaks are damped out. Overall, the inlet temperature that better approximates the experimental wall heat flux seems to be T_h = 1620 K, which can be considered as valid boundary conditions for future investigations. The comparison of the wall heat fluxes for this experiment shows a double validation. Because the numerical simulations provide values close

to the reconstructed q_w, the method of Dalshad et al. [11] as well as the laminar chemistry combustion model could both be validated for this configuration.

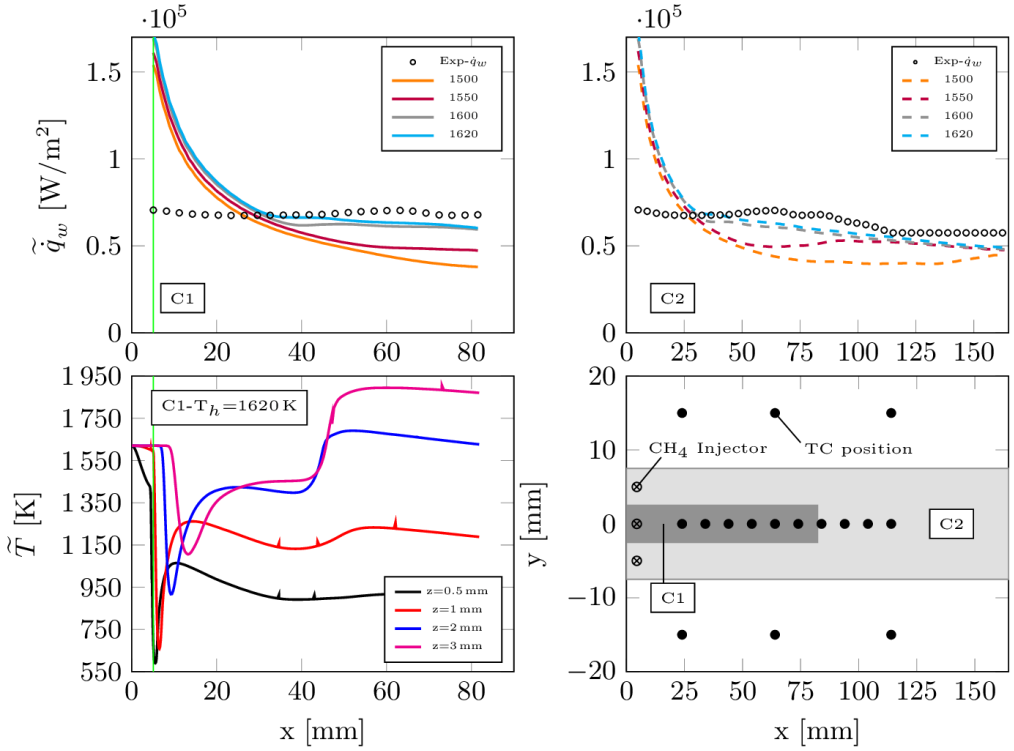

Figure 7. Top: wall heat flux predictions for configurations C1 and C2. Bottom: thermal boundary layer and thermocouple positions at wall.

Conclusions

Laminar finite rate chemistry LES were used in this work to investigate a selected configuration of a novel test bench featuring near-wall secondary reactions of methane in an oxidizer-rich crossflow. A parametric study involving a variation in grid refinement, reaction mechanism, turbulent inflow, hot gas inlet temperatures as well as the interaction between the fuel jets was presented. OH-PLIF images and wall heat flux reconstruction available from the experiment were used to qualitatively locate the autoignition length and to assess the thermal loads in the LES.

The LES computations were capable to detect the double flame structure observed from the OH-PLIF images. The dependency of the autoignition length on grid refinement, chemical mechanism and oxidizer inlet temperature were investigated without a turbulent content for the hot crossflow. The autoignition length estimated from the OH and CH_2O concentrations was strongly dependent on the temperature of the hot reactants. By increasing the temperature at the oxidizer inlet, the flame tip moved upstream towards the fuel injection nozzles. On the contrary, the grid refinement and the chemical mechanisms had a weak effect on the autoignition length. By enabling the turbulent content at the hot inlet, enhanced mixing caused a shift of the autoignition point further upstream, although minimal compared to the domain length. The effect of chemistry appeared to be stronger than turbulence, because in this configuration the fuel was injected with a high momentum ratio into the crossflow and the oxidizer stream was already reactive at the given temperatures.

Regarding the thermal loads, the LES reported smoother local peaks than the experiment, the location depending on the temperature of the hot oxidizer. A high local peak was predicted by the simulations right after the injectors, which was not seen by the experiment. The numerical wall heat flux could not clearly identify the local peak due to the reaction zone close to the wall, although the thermal loads presented the same order of magnitude of the experiment downstream the fuel injection nozzles. A qualitatively good approximation with the autoignition length and the wall heat fluxes of the experiment was obtained for a hot inlet temperature of 1600-1620 K.

References

[1] Kirk D. R., Guenette G. R., Lukachko S. P., Waitz, I. A.: *Gas Turbine Engine Durability Impacts of High Fuel-Air Ratio Combustors-Part II: Near-Wall Reaction Effects on Film-Cooled Heat Transfer*, J. Eng. Gas Turbines Power 125, 3,751-759, 2003.

[2] Lukachko S. P., Kirk D. R., Waitz I. A.: *Gas Turbine Engine Durability Impacts of High Fuel-Air Ratio Combustors_Part I: Potential for Secondary Combustion of Partially Reacted Fuel*, J. Eng. Gas Turbines Power 125, 3, 742-750, 2003.

[3] Evans D. S.: *The Impact of Heat Release in Turbine Film Cooling*, 47th AIAA Aerospace Sciences Meeting including The New Horizons Forum and Aerospace Exposition, 2009.

[4] Richardson D., Jiang N., Blunck D., Gord J., Roy S.: *Characterization of inverse diffusion flames in vitiated cross flows via two-photon planar laser-induced fluorescence of CO and 2-D thermometry*, Combustion and Flame, 168:270–285, 2016.

[5] Polanka M., Zelina J., Anderson W., Sekar B., Evans D., Lin C., Stouffer, S.: *Heat Release in Turbine Cooling I: Experimental and Computational Comparison of Three Geometries*, J. Propuls. Power 27, 2, 257-268, 2011.

[6] Ghasemi E., Soleimani S., Lin, C.: *Secondary reactions of turbulent reacting flows over a film-cooled surface*. International Communications in Heat and Mass Transfer 55, 93-101, 2014.

[7] Pohl S., Frank G., Pfitzner M.: *Heat Transfer In Reacting Cooling Films, Part I: Influence and Validation of Combustion Modelling in CFD Simulations*, Proceedings of ASME Turbo Expo 2014: Turbine Technical Conference and Exposition, 2014.

[8] Frank G.: *Reaktive Kühlfilme und Flamme-Wand-Interaktionen in Raketenbrennkammern*, PhD thesis, Bundeswehr University of Munich, 2018.

[9] Dalshad R., Sander T., Pfitzner M.: *Characterization of a newly designed test bench for investigation of flame-wall-interaction*, Proc. of the ASME Turbo Expo 2021, GT2021-59170, 2021.

[10] Dalshad R., Sander T., Pfitzner M.: *Experimental investigation of autoignition in non-premixed gaseous CH4/hot air cross flows*, 29. Deutscher Flammentag, 2019.

[11] Dalshad R., Perakis N., Pfitzner M., Haidn, O.: *Implementation of an Optimization Method for Inverse Heat Conduction and Sensor Position Correction*, Comsol Conference 2020 User Presentations, 2020.

[12] Breda P, Fischer L., Dalshad R., Pfitzner M.: *Numerical characterization of a novel test bench featuring CH4 secondary reactions*, in peer-review at Aerosp. Sci. Technol., June 2021.

[13] Pope S.: *Ten questions concerning the large-eddy simulation of turbulent flows*, New J. Phys. 6, 35, 1, 2004.

[14] Nicoud F., Ducros F.: *Subgrid-Scale Stress Modelling Based on the Square of the Velocity Gradient Tensor*, Flow Turbul. Combust. 62, 3, 183-200, 1999.

[15] Hansinger M., Zirwes T., Zips J., Pfitzner M., Zhang F., Habisreuther P., Bockhorn H.: *The Eulerian Stochastic Fields method applied to Large Eddy Simulations of a piloted flame with inhomogeneous inlet*, Flow Turbul. Combust. 105, 837–867, 2020.

[16] Breda P., Hansinger M., Pfitzner M.: *Chemistry computation without a subgrid PDF model in LES of turbulent non-premixed flames showing moderate local extinction*, Proc. Combust. Inst., 38, 2, 2655–2663, 2021.

[17] Lampmann A., Hansinger H., Pfitzner M.: *LES of a turbulent CH4/air multi-regime burner configuration using an artificially thickened flame model with reduced finite-rate chemistry*, 10th European Combustion Meeting, April 2021.

[18] Immer M.C.: *Time-resolved measurement and simulation of local scale turbulent urban flow*. PhD thesis, ETH Zürich, 2016.

[19] Lu T., Law C.: *A Directed Relation Graph Method for Mechanism Reduction*, Proc. Combust. Inst. 30, 1, 1333-1341, 2005.

[20] Lu T., Law C.: *A criterion based on computational singular perturbation for the identification of quasi steady state species: A reduced mechanism for methane oxidation with NO chemistry*. Combust. Flame 154, 4, 761-774, 2008.

[21] Markides C.N., Mastorakos E.: *An experimental study of hydrogen autoignition in a turbulent co-flow of heated air*, Proc. Combust. Inst., 30, 1, 883–891, 2005.